International Journal of Climatology

International Journal of Climatology RMetS

RESEARCH ARTICLE

Influence of Anthropogenic Activities on Near-Surface Wind Speed Attenuation Over the Tibetan Plateau

Lihua Zhu[1] | Wei Hua[1] | Gang Huang[2,3] | Ye Wang[4]

[1]School of Atmospheric Sciences/Climate Change and Resource Utilization in Complex Terrain Regions Key Laboratory of Sichuan Province, Chengdu University of Information Technology, Chengdu, China | [2]State Key Laboratory of Earth System Numerical Modeling and Application, Institute of Atmospheric Physics, Chinese Academy of Sciences, Beijing, China | [3]University of Chinese Academy of Sciences, Beijing, China | [4]School of Mathematics and Statistics, Henan University, Kaifeng, China

Correspondence: Wei Hua (huawei@cuit.edu.cn)

Received: 16 November 2025 | **Revised:** 31 December 2025 | **Accepted:** 28 January 2026

Keywords: anthropogenic activities | greenhouse gases | long-term trend | near-surface wind speed | Tibetan Plateau

ABSTRACT

A comprehensive understanding of long-term trends in near-surface wind speed (SWS) and their underlying physical mechanisms is imperative for progress in atmospheric science, climatology, and energy-related fields. Utilising observational data and simulations from 10 models, this study investigates the role of anthropogenic activities in the observed decline of SWS over the Tibetan Plateau (TP) from 1961 to 2014. The results show a widespread and statistically significant decline in the annual mean SWS across the TP. The models qualitatively captured this decreasing trend under all-forcing scenarios. Detection and attribution analysis attributes the observed wind speed decline primarily to anthropogenic forcings, which account for most of the reduction, while natural forcings show no detectable influence. Among these anthropogenic factors, greenhouse gas (GHG) emissions were responsible for the greatest decrease in SWS over the TP. In comparison, the contributions from aerosol forcing and land use change were marginal; their negative regression coefficients indicate that they partially offset the overall weakening trend. The underlying mechanism involves GHG-induced asymmetric warming. This warming weakened the pressure gradient over the TP by causing a greater increase in geopotential height over the mid-high latitudes north of the plateau than over the regions to its south. These findings highlight the dominant influence of human activities on wind speed changes over the TP, with important implications for wind resource planning and ecological management.

1 | Introduction

Near-surface wind speed (SWS) over terrestrial environments serves as a fundamental component of atmospheric circulation, exerting a major influence on the distribution and flux of energy and substances within the lower atmosphere. Fluctuations in SWS exert profound effects on a diversity of environmental and climatic domains, including but not limited to: hydrological cycles (Liu et al. 2014), regional evapotranspiration rates (McVicar et al. 2012; McMahon et al. 2013), ambient air quality (Cai et al. 2017; Han et al. 2017; Zhang et al. 2020), the occurrence of dust storms (Wang et al. 2017), and the viability of wind power generation (Tian et al. 2019; Zeng et al. 2019; Pryor and Barthelmie 2021). Consequently, elucidating the variability inherent to SWS is a subject of considerable scientific interest.

Under global warming, significant declines in wind speeds have been documented across terrestrial regions (Wu et al. 2018; Tian et al. 2019). Internal climate variability and external forcings can both affect the changes in SWS (Wu et al. 2018). From the perspective of internal climate variability, the North Atlantic Oscillation (NAO) is found to partly account for fluctuations in

SWS across multiple regions (Earl et al. 2013; Jerez et al. 2013; Azorin-Molina et al. 2014, 2016). The arctic oscillation (AO) has significant influence on the distribution of changes in SWS over China (Chen et al. 2013). The Interdecadal Pacific Oscillation (IPO) modulates regional wind speed variability on decadal timescales (Fu et al. 2011). In terms of external forcings, anthropogenic (ANT) forcing contributed particularly to the long-term reduction in SWS (Zha et al. 2024). The warming influence of increased atmospheric greenhouse gas (GHG) concentrations and the cooling influence from atmospheric aerosols (AER) have dominated changes in climate system drivers since 1750 (IPCC 2021). Elevating GHG and AER concentrations directly influence radiative forcing and determine the magnitude of warming when combined with associated climate feedbacks (Kramer et al. 2021; Li et al. 2022), with the warming displaying significant spatial heterogeneity globally (Seneviratne et al. 2016; IPCC 2021). Anthropogenically induced warming and cooling anomalies (from GHGs and AERs) modify regional thermal contrasts, thereby altering pressure gradients and subsequently influencing surface wind regimes (You et al. 2010; Clifton and Lundquist 2012; Lin et al. 2013; Zhang and Li 2016). Meanwhile, changes in surface roughness induced by land-use and land-cover change partially explain observed variations in SWS (Vautard et al. 2010; Zha et al. 2017). In general, changes in SWS result from combined effects of ANT activities and natural climate variability. Under global warming, quantifying the contribution from human activities remains critically important yet insufficiently understood. The weighting of different ANT drivers (e.g., land-use change [LUC], AER emissions) in altering surface wind regimes varies considerably across geographical regions (Wu et al. 2018). Attribution analyses should be conducted regionally.

The Tibetan Plateau (TP), renowned as the 'Roof of the World' and 'the Water Tower of Asia', possesses the most abundant wind energy resources in China (Gao et al. 2020). Changes in SWS play a pivotal role not only in wind energy potential but also in regulating the hydrological cycle and shaping local geomorphology and ecosystems (Yang et al. 2014; Dong et al. 2017; Song et al. 2017; Gao et al. 2020). SWS over the elevated TP have declined more significantly than those in other regions of China (McVicar et al. 2010; You et al. 2010), and attracting increasing attention (Kuang and Jiao 2016; Ding et al. 2021; Guo and Tian 2022; Ma et al. 2024; Zhang, Azorin-Molina, et al. 2024). However, it remains unclear to what extent ANT activities have contributed to the observed SWS decline over the TP under global warming. Moreover, the relative impacts of different ANT forcing components—particularly GHGs, AERs and LUC—on SWS attenuation over the TP remain poorly quantified. Therefore, using outputs from the Coupled Model Intercomparison Project Phase 6 (CMIP6) and observations, this study employs correlation-based detection and attribution analyses, combined with multivariate linear regression, to quantify the contributions of different external forcings to the observed decline in SWS over the TP during 1961–2014. The findings are expected to advance the understanding of regional climate change mechanisms on the TP and provide a scientific basis for formulating policies related to wind energy development, ecological protection and sustainable land use management in this unique and vital region.

2 | Materials and Methods

2.1 | Observations and CMIP6

This study used monthly 10-m wind speed data from the gridded observational dataset over China (CN05.1) to detect SWS changes (Wu and Gao 2013). The CN05.1 dataset is derived from quality-controlled observations at over 2400 meteorological stations across China, has a spatial resolution of $0.25° \times 0.25°$ and covers the period from 1961 to present (Wu and Gao 2013; Wu et al. 2017). The CN05.1 dataset employs an anomaly-based interpolation scheme to convert station data into a gridded format, a methodology consistent with that of the Climatic Research Unit (CRU) dataset (New et al. 2002; Xu et al. 2009). This two-stage procedure first constructs a baseline climatological field using thin-plate smoothing spline interpolation. It then interpolates daily station anomalies to the grid via angular distance weighting. The final gridded product is obtained by superimposing the daily anomaly field onto this climatological background (Shi et al. 2018; Wu and Gao 2013). Spatial interpolation in the CN05 dataset leverages the flexibility of spline functions, which can incorporate covariate sub-models—for example, to account for how variables vary with elevation—thereby enhancing accuracy. Specifically, thin-plate splines utilise longitude and latitude as primary variables, with elevation integrated as a covariate to interpolate the baseline climatic fields (Wu and Gao 2013). This method is particularly robust for sparse or irregularly distributed data points (New et al. 2002). This study utilised the aforementioned datasets for the TP covering the period 1961–2014. The CN05.1 dataset has been widely employed for analysing climate changes over the TP and verifying the output of climate model simulations (Jiang and Zhou 2023; Li et al. 2023; Wang et al. 2023; Liu et al. 2024; Xiang et al. 2024; Wu et al. 2025).

We used outputs from 10 models of the CMIP6 (Eyring et al. 2016) to assess the influence of ANT activities on SWS attenuation over the TP. Details of the models are provided in Table 1. We utilised historical simulations to estimate the SWS responses to different external forcings, including all external forcings (ALL), natural-only runs (NAT), GHG forcings only, AER-only runs and land-use-unchanged runs (noLUC). As performed in many studies, the response to LUC forcing was estimated by comparing differences between the ALL and noLUC experiments (Liu et al. 2022; Luo et al. 2024; Zhang, Gao, et al. 2024). The former is driven by historical evolving natural (e.g., orbital, solar and volcanic) and ANT (e.g., GHGs, AERs and LUC) forcings (Eyring et al. 2016), while the latter experiment is identical to the former except that all land-use and land-cover are fixed at the 1850 level during the historical simulation from 1850 to 2014 (Lawrence et al. 2016). Similarly, the response to ANT forcing was estimated by subtracting NAT forcings from ALL forcings (Hu et al. 2020; Paik and Min 2020; Seong et al. 2021; Xu et al. 2022; Pan et al. 2023). To ensure equal weighting across models, the multimodel ensemble mean is derived by taking the mean of each model's ensemble and then averaging across all models. To quantify natural internal climate variability, preindustrial control (piControl) simulations were employed, wherein GHG concentrations, AER loading, ozone levels and solar irradiance were fixed at preindustrial levels throughout the

TABLE 1 | Summary of CMIP6 models, experiments and ensemble members employed in this study.

No.	Models	Historical	Hist-NAT	Hist-AER	Hist-GHG	Hist-noLUC	piControl
1	ACCESS-CM2	10	3	1	1	—	9
2	BCC-CSM2-MR	1	1	1	2	1	11
3	CESM2	9	2	1	1	2	22
4	CanESM5	10	10	10	5	8	37
5	CNRM-CM6-1	5	5	5	5	—	9
6	E3SM-2-0	10	5	3	3	——	9
7	HadGEM3-GC31-LL	2	10	3	3	—	37
8	IPSL-CM6A-LR	4	4	10	8	3	18
9	MIROC6	5	5	10	5	—	14
10	NorESM2-LM	2	3	3	2	1	14
	Sum (models)	58 (10)	48 (10)	47 (10)	35 (10)	15 (5)	180 (10)

Note: Parentheses in the last row show the total number of models for each forcing.

simulation. For consistency with observational records, this study focuses on historical simulations spanning the 1961–2014 period.

2.2 | Correlation-Based Detection and Attribution Analyses

Monthly anomalies of observations and external forcing simulations were calculated for each grid point relative to the 1961–1990 baseline period. The study focuses on the TP (25°–40° N, 75°–105° E), a region with an altitude exceeding 2000 m. To assess the possible influence of external forcings on SWS changes, we employed a correlation-based detection method that has been widely applied in previous studies (Qian and Zhang 2015; Wan et al. 2015; Zhu et al. 2022). Detection and attribution analyses were performed for regional mean SWS anomalies above 2000 m elevation over the TP using non-overlapping 5-year means from 1961 to 2014 to filter out the interannual oscillation signal. Model-simulated responses to ALL, NAT, ANT, GHG, AER and LUC forcings were compared with observations to identify observational evidence of climate responses to different external forcings. The piControl simulations were segmented into multiple non-overlapping intervals matching the duration of observations and historical runs, with identical processing methods applied to all forced simulations. Correlation coefficients were calculated between observations and model-simulated forced responses to the specified external forcings. To assess statistical significance, parallel correlations were calculated between observations and each of the 180 piControl simulation segments. A one-sided Monte Carlo test was applied to evaluate the statistical significance of the correlation. If the correlation coefficient between observations and an externally forced signal exceeded the 90th percentile of the correlation coefficients between the observations and the piControl intervals, the relationship was deemed statistically significant at the 90% confidence level relative to internal variability, indicating detectable forced responses in observations.

2.3 | Contributions of External Forcings

To assess the relative contributions of different external forcings to interdecadal wind speed variations, we employed a multivariate linear regression approach, expressed as

$$y = \sum_{i=1}^{m} \beta_i X_i + \varepsilon \quad (1)$$

where y denotes the observation vector, β_i is the regression coefficient for the ith external forcing, X_i represents the simulated climate response to that forcing and ε is the residual term. Two regression models were developed: the NAT-ANT model was designed to quantify the contributions of natural and ANT forcings and the GHG-AER-LUC model was designed to separate the effects of GHGs, AERs and LUC. The relative contribution of each external forcing was calculated as follows:

$$\text{Contribution}_i = \beta_i \Delta X_i \quad (2)$$

where β_i is the regression coefficient for the ith forcing, and ΔX_i denotes the change in SWS under that forcing over the period 1961–2014.

3 | Results

3.1 | Decreased SWS Over the TP

Annual mean SWS across the TP exhibits a significant and spatially extensive declining trend from 1961 to 2014 (Figure 1a). The decadal-scale variability demonstrates notable spatial coherence, with most grid cells showing a strong positive correlation with the regionally averaged wind speed (Figure 1b). The 10th–90th percentile range of the grid cells reflects substantial interannual spread in SWS values. Nevertheless, a coherent and persistent declining trend is apparent across the entire region over the study period (Figure 1c), with a mean rate of decrease

of $-0.116\,m\,s^{-1}$ decade^{-1} ($p < 0.01$). This high spatial coherence indicates that the temporal evolution of SWS is largely uniform across the plateau, justifying the use of a regional mean time series for subsequent detection analysis.

Simulations from the 10 CMIP6 models are broadly consistent with the observed historical decline in SWS over the TP (Figure 2a). All selected models successfully capture the negative trend qualitatively (Figure 2b), and the multi-model mean

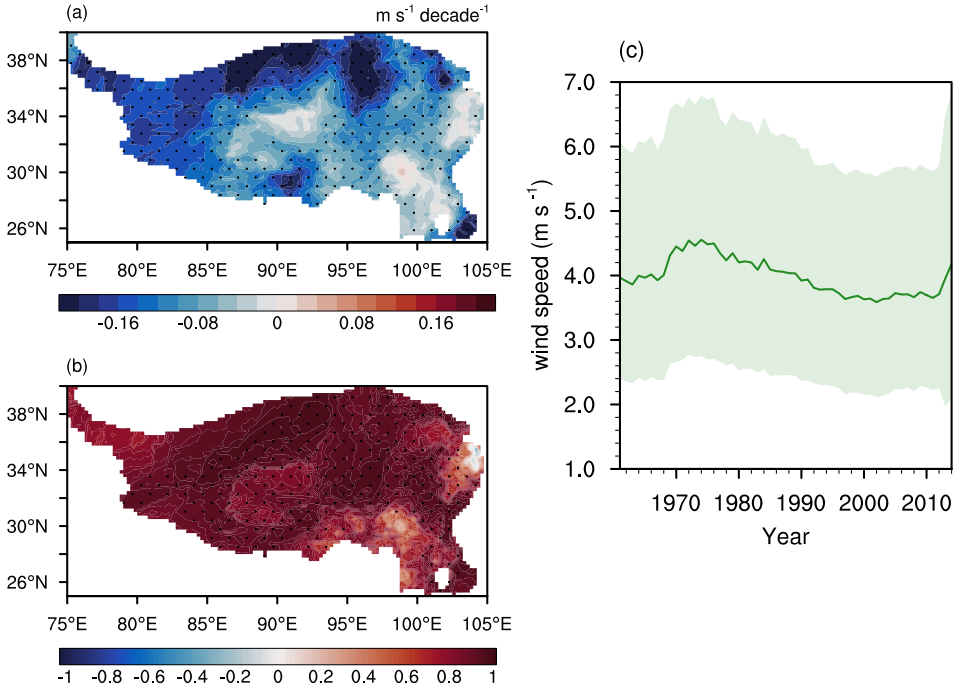

FIGURE 1 | (a) Trends in annual mean 10-m wind speed over the Tibetan Plateau (TP; elevation > 2000 m) from 1961 to 2014, based on observations. Dots denote grid points where the trends are statistically significant ($p < 0.10$). (b) Spatial pattern of correlation coefficients between the TP-wide average and each grid point for the 5-year running mean of annual 10-m wind speed. Dots indicate where the correlation coefficients are significant ($p < 0.10$), accounting for the effective degrees of freedom. (c) Temporal evolution of annual 10-m wind speed over the TP (elevation > 2000 m). The shading indicates the 10th–90th percentile range across individual grid cells. [Colour figure can be viewed at wileyonlinelibrary.com]

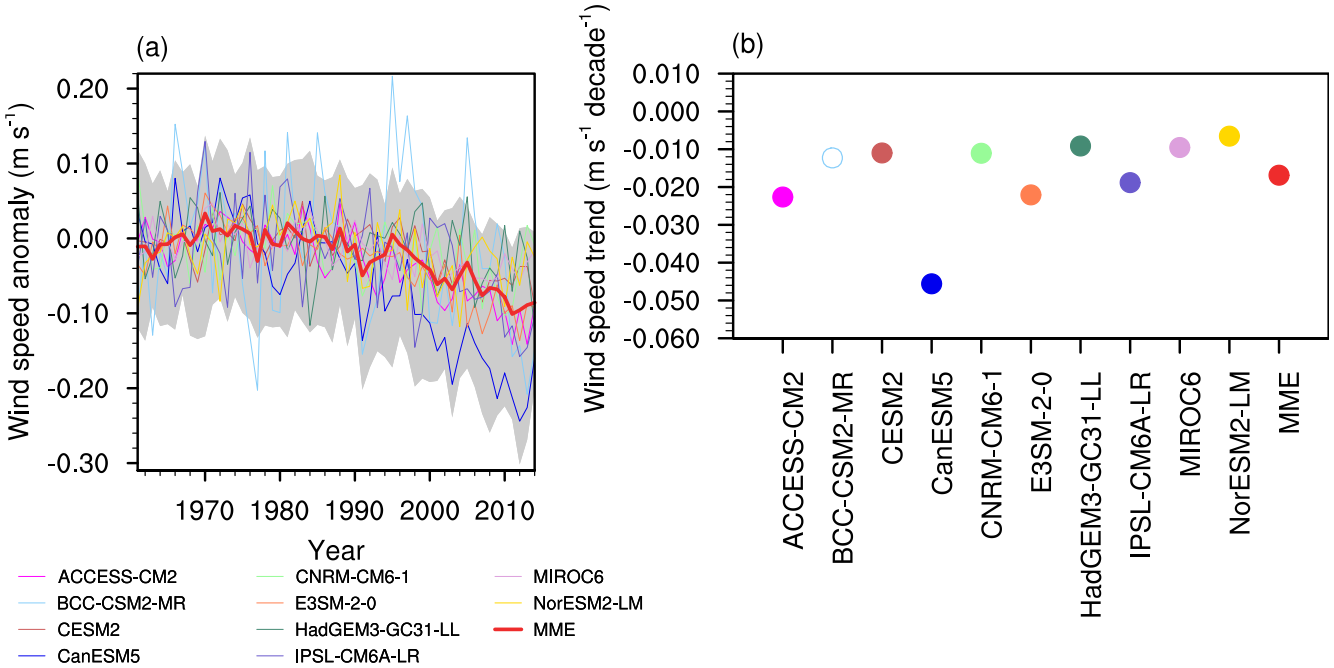

FIGURE 2 | (a) Anomalies of 10-m wind speed over the TP (elevation > 2000 m) during 1961–2014 relative to the 1961–1990 baseline period, derived from CMIP6 multi-model simulations. The grey shading represents the intermodel spread (10th–90th percentile range) across 58 ensemble members under ALL forcing. (b) Linear trends of 10-m wind speed during 1961–2014 for individual models and the multi-model ensemble mean. Solid circles denote trends that are statistically significant at the 90% confidence level. [Colour figure can be viewed at wileyonlinelibrary.com]

produces a statistically significant trend of $-0.017\,m\,s^{-1}$ decade^{-1} ($p<0.01$). This demonstrates that the models generally replicate the observed phenomenon, albeit with an underestimation of its magnitude.

3.2 | Influence of ANT Activities on SWS Attenuation

To detect the contribution of ANT activities to the decreased SWS over the TP, a correlation-based detection and attribution analysis has been performed here using ensemble members from 10 CMIP6 models. The observed overall decline in SWS is well captured by simulations incorporating ALL forcings (both ANT and NAT) as well as those with ANT forcing alone (Figure 3a). In contrast, simulations driven by NAT forcing alone fail to reproduce the observed weakening trend. This implies that ANT forcings are the primary driver of the observed decline in wind speed in the ALL simulations. This conclusion is strongly supported by the significant decreasing trend of $-0.018\,m\,s^{-1}$ decade^{-1} ($p<0.01$) simulated under ANT forcing alone. Further supporting this, the correlation coefficients between observations and simulated responses are 0.693 for ALL, 0.725 for ANT and only 0.046 for NAT forcings (Figure 3b). A one-sided Monte Carlo test based on piControl simulations confirms that the correlations for ALL and ANT forcings are statistically significant ($p<0.01$), whereas that for NAT forcing is not. Thus, the simulated responses to ALL and ANT forcings are detectable, while the response to NAT forcing is not.

Furthermore, compared to the trends under AER and LUC forcings, the decreasing trend in SWS under GHG forcing is much closer to the observed trend, with a rate of $-0.013\,m\,s^{-1}$ decade^{-1} ($p<0.01$; Figure 3c). The correlation between observations and the simulated response to GHG forcing is statistically significant ($r=0.757$, $p<0.01$), as confirmed by a one-sided Monte Carlo

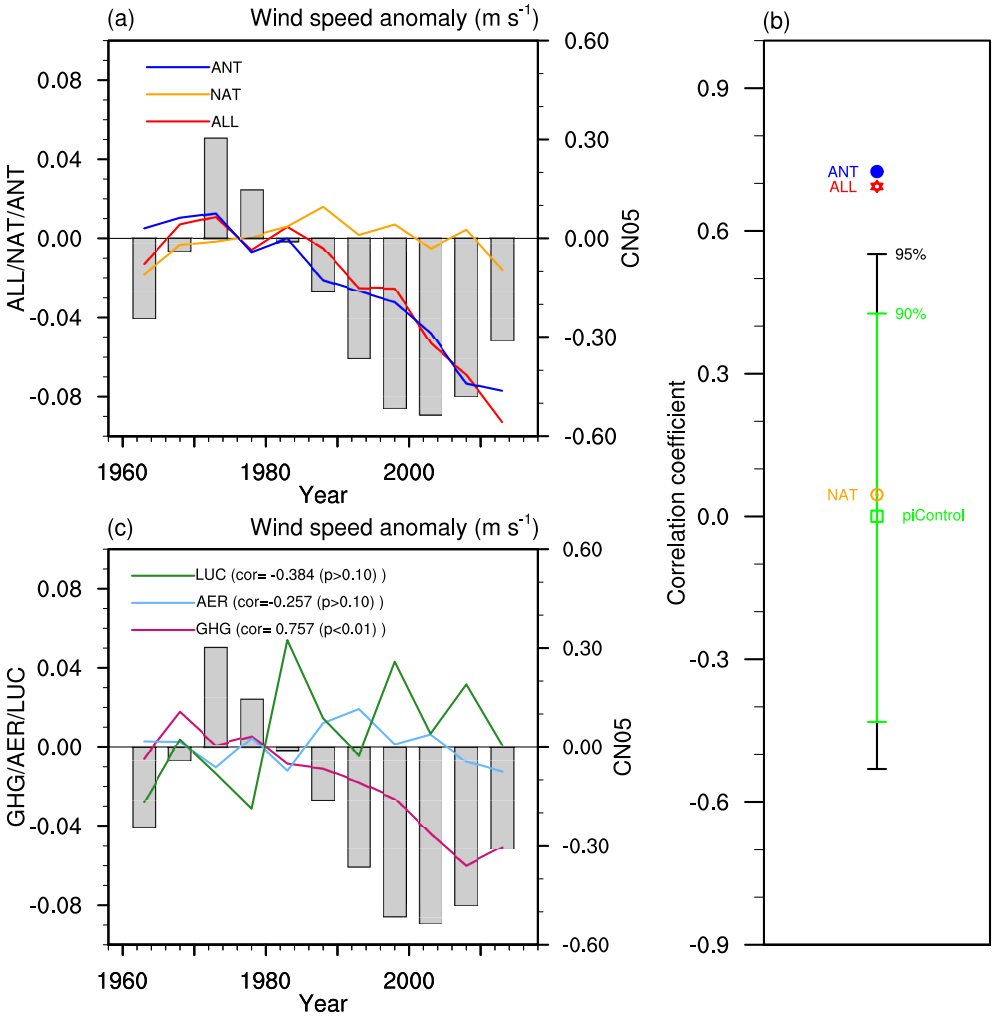

FIGURE 3 | Five-year non-overlapping mean anomalies of SWS over the TP above 2000 m from observations (CN05; bars) and CMIP6 model simulations under (a) all-forcing (ALL), natural-only (NAT) and anthropogenic-only (ANT) forcings and (c) greenhouse gas-only (GHG), anthropogenic aerosol-only (AER) and land-use change (LUC) forcings. Anomalies are estimated for the 1961–1990 baseline period. (b) Correlation coefficients between observed and model-simulated SWS over the TP. Red asterisks, blue solid circles and orange hollow circle denote correlation coefficients between the observations and model-simulated responses to ALL forcing, ANT forcing and NAT forcing, respectively. The 5th–95th and 10th–90th percentile ranges of the correlation coefficients between the observations and 180 segments of piControl simulations are expressed by black error bars and green error bars, respectively. [Colour figure can be viewed at wileyonlinelibrary.com]

test. In contrast, the correlations for AER ($r = -0.257$) and LUC ($r = -0.384$) forcings are not significant, even at the 0.10 level. This lack of robust statistical relationships rules out a significant contribution from AERs or LUC to the reduction in SWS. Therefore, the detectable decline in the ANT response is primarily attributable to GHG forcing.

The influence of GHG on the decline in SWS is further confirmed through spatial analysis. When comparing the observed trends with those from the CMIP6 historical experiments, it is evident that the models successfully capture the spatial pattern of wind speed changes over the TP, demonstrating a statistically significant pattern correlation of 0.336 ($p < 0.10$; Figure 4a). In contrast to the contribution from NAT forcing (Figure 4b), the decreasing pattern of SWS under ALL forcing is primarily attributable to ANT forcing (Figure 4c). This reinforces the notion that ANT factors have played a significant role in shaping the recent wind speed changes over the TP. Specifically, the weakening of wind speed in the ANT forcing runs is predominantly driven by GHG forcing (Figure 4d), while the contribution from AER forcing is relatively minor (Figure 4e). Conversely, LUC forcing alone induces a significant increase in wind speed across most of the TP (Figure 4f), indicating a partial offset to the overall weakening trend. These findings suggest that human activities, particularly GHG emissions, are the principal contributor to the observed prevailing decline in SWS over the TP during the period 1961–2014.

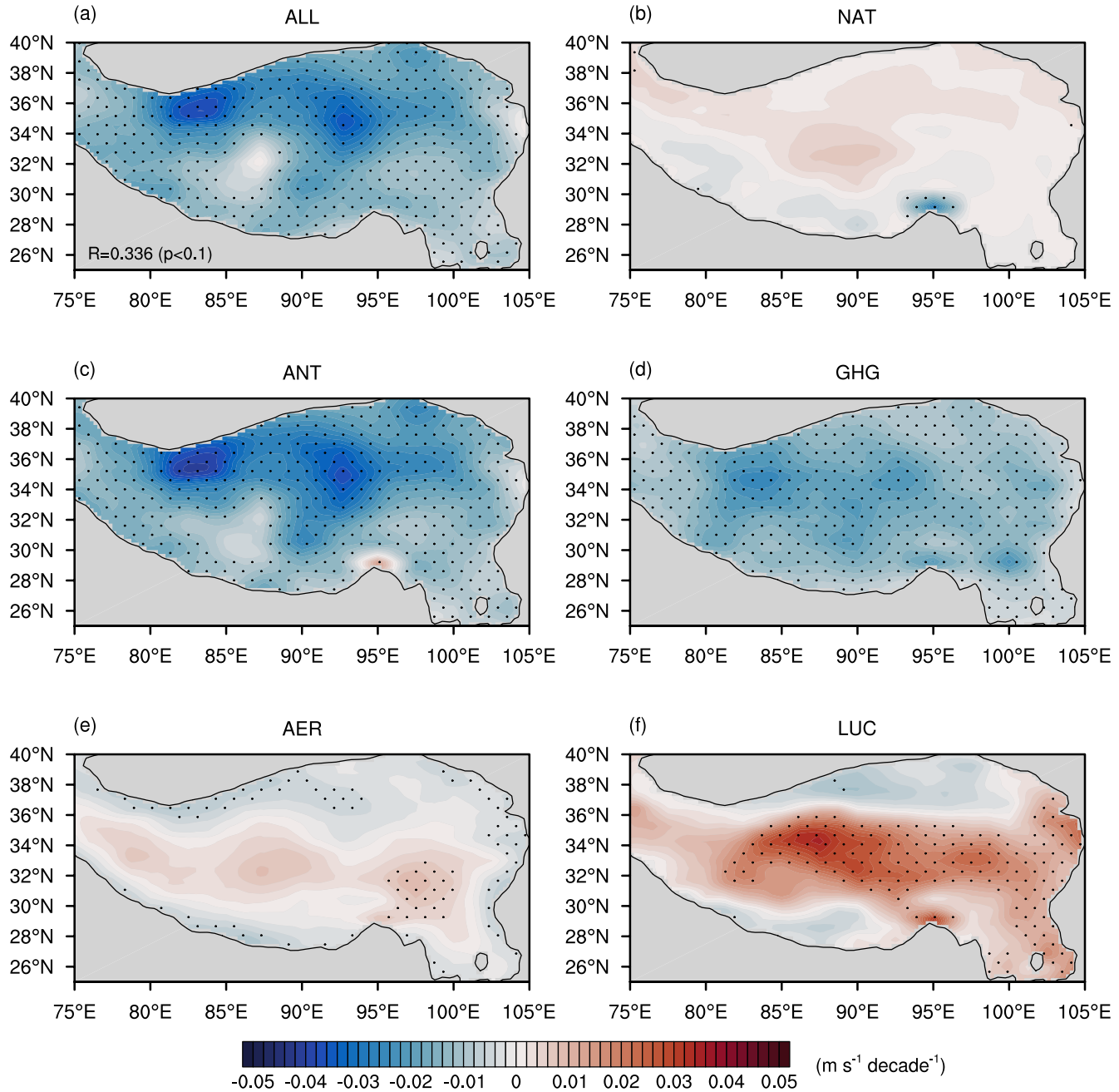

FIGURE 4 | Linear trends of the SWS over the TP during 1961–2014 in the model-simulated responses to the (a) ALL, (b) NAT, (c) ANT, (d) GHG, (e) AER and (f) LUC forcings. The multimodel ensemble mean is shown. Dots mark where the trends are significant at the 0.05 level. The elevation of 2000 m is used as the outline of TP. [Colour figure can be viewed at wileyonlinelibrary.com]

A multiple linear regression was performed to quantify the contributions of NAT and ANT forcings, the latter further decomposed into GHG, AER and LUC, to the observed decrease in SWS. Based on the NAT-ANT multivariate linear regression model ($p < 0.10$), the analysis attributes a reduction of −0.605 m/s (90% confidence interval: −0.226 to −0.983 m/s) out of the observed total decline of −0.628 m/s during 1961–2014 to ANT forcing (Figure 5), while the contribution from NAT forcing is negligible. Further decomposition of the ANT forcing using the GHG-AER-LUC regression model ($p < 0.01$) indicates that among the three individual components of ANT forcing, GHG forcing accounts for a decrease of −0.628 m/s (90% confidence interval: −0.354 to −0.902 m/s; Figure 5). In contrast, the contributions from AER (0.027 m/s) and LUC (−0.110 m/s) are minor. Their negative regression coefficients imply that both forcings actually exert a mitigating effect on the overall decline in wind speed. This contribution analysis based on multiple linear regression further verifies the dominant role of GHG forcing in the weakening of SWS over the TP.

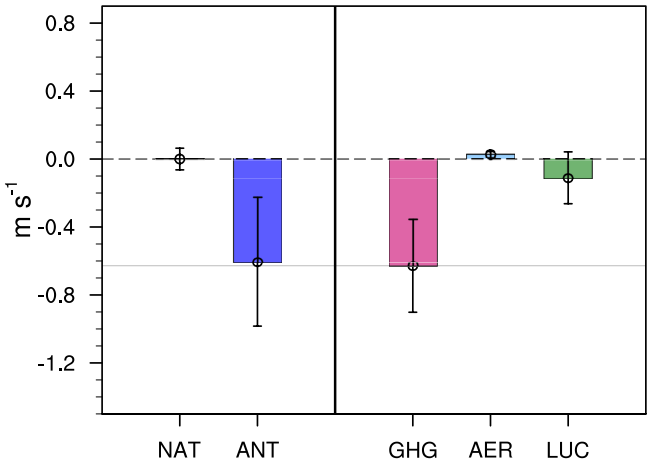

FIGURE 5 | Attributable reduction in SWS over the TP due to NAT and ANT forcings and due to GHG, AER and LUC forcings from the multiple-variable linear regression, along with their 90% confidence intervals. The solid line indicates the observed decreasing magnitude of SWS from 1961 to 2014. [Colour figure can be viewed at wileyonlinelibrary.com]

3.3 | GHG-Induced Asymmetric Warming

From the above, it is concluded that the decreased SWS over the TP is mainly attributed to human activities, especially to GHG forcing. One of the possible impact pathways of GHG on wind change is regional differences in warming, which can affect pressure gradients and therefore wind speed. To demonstrate the cause of the attenuated wind speed over the TP, the spatial

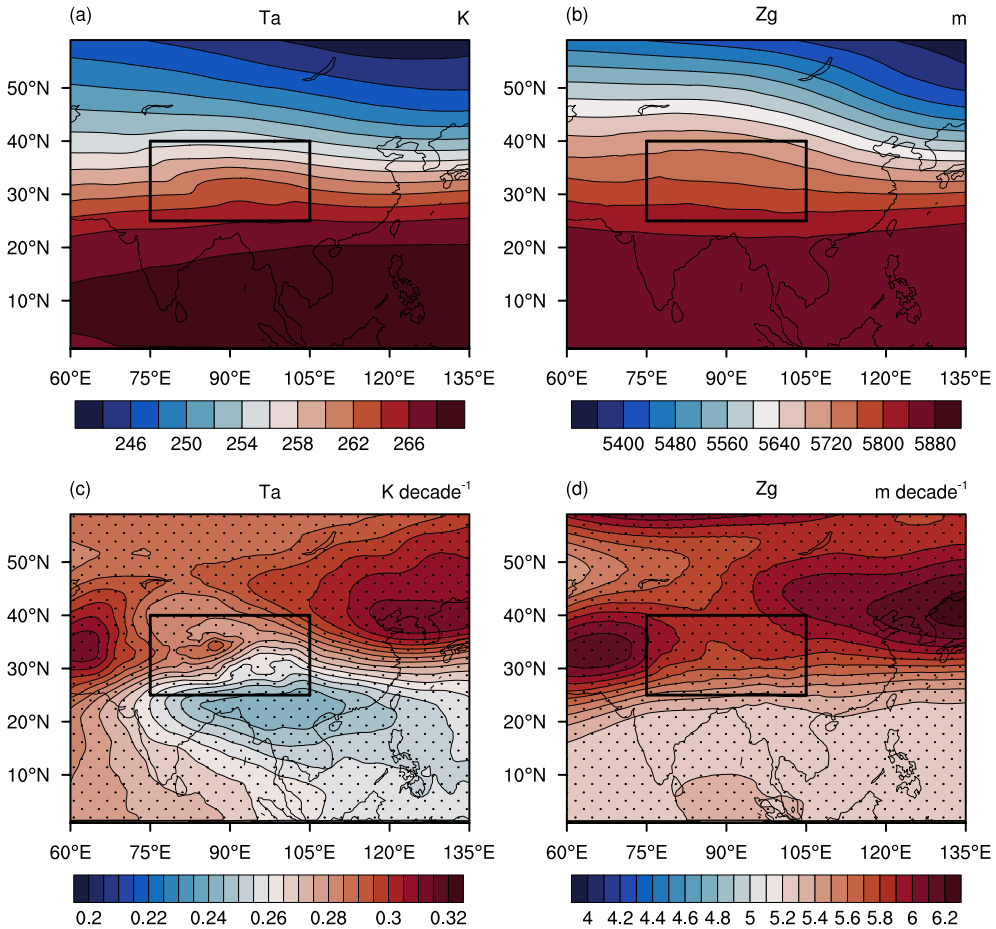

FIGURE 6 | Spatial distribution of the climatological mean and trend of (a, c) air temperature and (b, d) geopotential height at 500 hPa from the GHG-only forcing experiment for the period 1961–2014. Dots mark locations where the trends are significant at the 0.05 level. The black rectangle denotes the TP area. [Colour figure can be viewed at wileyonlinelibrary.com]

distributions of the climatological mean and trend of air temperature and geopotential height at 500 hPa under GHG forcing for the period 1961–2014 have been analysed here. On average, both air temperature (Figure 6a) and geopotential height (Figure 6b) over the TP exhibit a pronounced south-to-north gradient. Under GHG forcing, more pronounced warming occurred in the mid-to-high latitudes northwest of the plateau compared to the low-latitude regions to its southeast (Figure 6c). This asymmetric warming induced a greater rise in geopotential height over the mid- to high-latitudes north of the TP than to the south (Figure 6d), thereby weakening the pressure gradient and leading to a decrease in SWS.

4 | Conclusions and Discussion

Based on observations and an ensemble of 10 CMIP6 model simulations, this study assesses the ANT influence on long-term SWS trends over the TP during the period 1961–2014. A robust and spatially coherent decrease in SWS over the TP from 1961 to 2014 is evident in observational data, thereby confirming the recently reported declining trend in homogenised annual wind speed over the TP (Zhang, Azorin-Molina, et al. 2024). CMIP6 model simulations attribute the observed wind speed decline primarily to ANT forcings, which explain most of the reduction (−0.605 out of −0.628 m/s), whereas natural forcings show no detectable influence. This result underscores the dominant role of human activities. Among ANT factors, GHG emissions are the leading contributor to wind speed attenuation. In contrast, the contributions from AER and LUC are marginal; moreover, their negative regression coefficients indicate they slightly mitigate the overall decline. This study therefore confirms the predominant role of GHG forcing in the recent weakening of surface winds over the region. The reduction in wind speed is mechanistically linked to GHG-driven warming disparities, which elevate geopotential height more markedly in regions north of the TP. The asymmetric warming pattern arises from a complex process that encompasses multiple factors, including snow/ice-albedo feedback, atmospheric circulation adjustment, temperature feedback, cloud feedback and water vapour feedback, among others (Dai et al. 2019; Overland and Wang 2010; Pithan and Mauritsen 2014; Screen and Simmonds 2010; Vavrus 2004; You et al. 2021). Consequently, the meridional pressure gradient—a critical driver of surface winds—is attenuated. These findings have important implications for understanding the regional climate system over the TP. By clarifying the roles of different ANT factors, we can better predict future trends of SWS changes and take targeted measures to mitigate the adverse impacts and make the most of the potential benefits.

A notable finding is that the CMIP6 multi-model mean, while qualitatively reproducing the observed declining trend in SWS, systematically underestimates its magnitude. This quantitative discrepancy is consistent with a recognised challenge in contemporary climate models, particularly over regions of complex topography (e.g., Jiang et al. 2024; Long et al. 2021; Shen et al. 2022). Potential contributing factors include the coarse resolution of global models, which smooths fine-scale terrain features, and uncertainties in the parameterization of boundary-layer processes and land-surface friction (e.g., Bichet et al. 2012; Jiang et al. 2024; Wu et al. 2020). Such a systematic bias underscores the need for caution when interpreting the quantitative aspects of future SWS projections derived from these models. It implies that the projected trends may also be subject to a similar level of uncertainty. Advancing model capabilities in representing local-scale processes, for instance through dynamical downscaling or improved parameterizations, is therefore crucial for reducing this uncertainty in regional climate projections (e.g., Dong et al. 2025; Jiménez et al. 2010; Zhou et al. 2018).

Author Contributions

Lihua Zhu: conceptualization, methodology, writing original draft, visualisation, formal analysis, validation. **Wei Hua:** resources, supervision, methodology. **Gang Huang:** supervision, methodology. **Ye Wang:** methodology.

Acknowledgements

We acknowledge the Climate Change Research Center, Chinese Academy of Sciences for providing the gridded observational dataset. We also thank the anonymous reviewers for their valuable comments and suggestions, which have helped improve the quality of this manuscript.

Funding

This work was supported by the National Natural Science Foundation of China (42575187, 42075019, 42105057), Sichuan Science and Technology Program (2025NSFSC2005) and the Second Tibetan Plateau Scientific Expedition and Research program (2019QZKK010203).

Conflicts of Interest

The authors declare no conflicts of interest.

Data Availability Statement

The gridded observational datasets are available from https://ccrc.iap.ac.cn/resource. The model outputs of CMIP6 community are available at https://esgf-node.llnl.gov/projects/cmip6/.

References

Azorin-Molina, C., J. A. Guijarro, T. R. McVicar, et al. 2016. "Trends of Daily Peak Wind Gusts in Spain and Portugal, 1961–2014." *Journal of Geophysical Research: Atmospheres* 121, no. 3: 1059–1078.

Azorin-Molina, C., S. M. Vicente-Serrano, T. R. McVicar, et al. 2014. "Homogenization and Assessment of Observed Near-Surface Wind Speed Trends Over Spain and Portugal, 1961–2011." *Journal of Climate* 27, no. 10: 3692–3712.

Bichet, A., M. Wild, D. Folini, and C. Schär. 2012. "Causes for Decadal Variations of Wind Speed Over Land: Sensitivity Studies With a Global Climate Model." *Geophysical Research Letters* 39, no. 11: L11701.

Cai, W., K. Li, H. Liao, H. Wang, and L. Wu. 2017. "Weather Conditions Conducive to Beijing Severe Haze More Frequent Under Climate Change." *Nature Climate Change* 7: 257–262.

Chen, L., D. Li, and S. C. Pryor. 2013. "Wind Speed Trends Over China: Quantifying the Magnitude and Assessing Causality." *International Journal of Climatology* 33, no. 11: 2579–2590.

Clifton, A., and J. K. Lundquist. 2012. "Data Clustering Reveals Climate Impacts on Local Wind Phenomena." *Journal of Applied Meteorology and Climatology* 51, no. 8: 1547–1557.

Dai, A. G., D. H. Luo, M. R. Song, et al. 2019. "Arctic Amplification Is Caused by Sea-Ice Loss Under Increasing CO_2." *Nature Communications* 10: 121.

Ding, J., L. Cuo, Y. Zhang, et al. 2021. "Varied Spatiotemporal Changes in Wind Speed Over the Tibetan Plateau and Its Surroundings in the Past Decades." *International Journal of Climatology* 41, no. 13: 5956–5976.

Dong, H., Y. Zhang, T. Tao, X. Du, Y. Zou, and S. Cao. 2025. "Sensitivity of Near-Ground Wind to PBL Schemes, Reanalysis Data, and Nudging in Month-Long WRF Simulations in the Tibetan Plateau With Highly Complex Terrain." *Atmospheric Research* 323: 108161.

Dong, Z., G. Hu, G. Qian, et al. 2017. "High-Altitude Aeolian Research on the Tibetan Plateau." *Reviews of Geophysics* 55, no. 4: 864–901.

Earl, N., S. Dorling, R. Hewston, and R. von Glasow. 2013. "1980–2010 Variability in U.K. Surface Wind Climate." *Journal of Climate* 26, no. 4: 1172–1191.

Eyring, V., S. Bony, G. A. Meehl, et al. 2016. "Overview of the Coupled Model Intercomparison Project Phase 6 (CMIP6) Experimental Design and Organization." *Geoscientific Model Development* 9, no. 5: 1937–1958.

Fu, G. B., J. J. Yu, Y. C. Zhang, et al. 2011. "Temporal Variation of Wind Speed in China for 1961–2007." *Theoretical and Applied Climatology* 104: 313–324.

Gao, Y., S. Ma, T. Wang, et al. 2020. "Assessing the Wind Energy Potential of China in Considering Its Variability/Intermittency." *Energy Conversion and Management* 226: 113580.

Guo, X., and L. Tian. 2022. "Spatial Patterns and Possible Mechanisms of Precipitation Changes in Recent Decades Over and Around the Tibetan Plateau in the Context of Intense Warming and Weakening Winds." *Climate Dynamics* 59: 2081–2102.

Han, Z., B. Zhou, Y. Xu, J. Wu, and Y. Shi. 2017. "Projected Changes in Haze Pollution Potential in China: An Ensemble of Regional Climate Model Simulations." *Atmospheric Chemistry and Physics* 17, no. 16: 10109–10123.

Hu, T., Y. Sun, X. Zhang, et al. 2020. "Human Influence on Frequency of Temperature Extremes." *Environmental Research Letters* 15, no. 6: 064014.

IPCC. 2021. "Climate Change 2021: The Physical Science Basis." https://www.ipcc.ch/report/ar6/wg1/downloads/report/IPCC_AR6_WGI_Full_Report.pdf.

Jerez, S., R. M. Trigo, S. M. Vicente-Serrano, et al. 2013. "The Impact of the North Atlantic Oscillation on the Renewable Energy Resources in Southwestern Europe." *Journal of Applied Meteorology and Climatology* 52, no. 10: 2204–2225.

Jiang, J., Y. Yu, Y. Zhou, et al. 2024. "Influence of Model Resolution on Wind Energy Simulations Over Tibetan Plateau Using CMIP6 HighResMIP." *Atmosphere* 15, no. 11: 1323.

Jiang, J., and T. Zhou. 2023. "Observational Constraint on the Contributions of Greenhouse Gas Emission and Anthropogenic Aerosol Removal to Tibetan Plateau Future Warming." *Geophysical Research Letters* 50, no. 17: e2023GL105427.

Jiménez, P. A., J. F. González-Rouco, E. García-Bustamante, et al. 2010. "Surface Wind Regionalization Over Complex Terrain: Evaluation and Analysis of a High-Resolution WRF Simulation." *Journal of Applied Meteorology and Climatology* 49, no. 2: 268–287.

Kramer, R. J., H. He, B. J. Soden, et al. 2021. "Observational Evidence of Increasing Global Radiative Forcing." *Geophysical Research Letters* 48, no. 7: e2020GL091585.

Kuang, X., and J. J. Jiao. 2016. "Review on Climate Change on the Tibetan Plateau During the Last Half Century." *Journal of Geophysical Research: Atmospheres* 121, no. 8: 3979–4007.

Lawrence, D. M., G. C. Hurtt, A. Arneth, et al. 2016. "The Land Use Model Intercomparison Project (LUMIP) Contribution to CMIP6: Rationale and Experimental Design." *Geoscientific Model Development* 9, no. 9: 2973–2998.

Li, J., B. E. Carlson, Y. L. Yung, et al. 2022. "Scattering and Absorbing Aerosols in the Climate System." *Nature Reviews Earth & Environment* 3: 363–379.

Li, P., X. Niu, Y. Mao, R. Wu, and X. Ling. 2023. "Assessment of Climate Simulation Over the Tibetan Plateau Based on High-Resolution Multi-RCM Within CORDEX-EA-II." *Atmospheric Research* 292: 106848.

Lin, C. G., K. Yang, J. Qin, et al. 2013. "Observation Coherent Trends of Surface and Upper-Air Wind Speed Over China Since 1960." *Journal of Climate* 26, no. 9: 2891–2903.

Liu, L., X. Gou, X. Wang, et al. 2024. "The Increases in Extreme Climatic Events Over the Northeastern Tibetan Plateau and Their Association With Atmospheric Circulation Changes." *Atmospheric Research* 304: 107410.

Liu, S., Y. Wang, G. J. Zhang, L. Wei, B. Wang, and L. Yu. 2022. "Contrasting Influences of Biogeophysical and Biogeochemical Impacts of Historical Land Use on Global Economic Inequality." *Nature Communications* 13: 2479.

Liu, X., X. J. Zhang, Q. Tang, and X.-Z. Zhang. 2014. "Effects of Surface Wind Speed Decline on Modeled Hydrological Conditions in China." *Hydrology and Earth System Sciences* 18, no. 8: 2803–2813.

Long, Y., C. Xu, F. Liu, Y. Liu, and G. Yin. 2021. "Evaluation and Projection of Wind Speed in the Arid Region of Northwest China Based on CMIP6." *Remote Sensing* 13, no. 20: 4076.

Luo, X., J. Ge, Y. Cao, et al. 2024. "Local and Nonlocal Biophysical Effects of Historical Land Use and Land Cover Changes in CMIP6 Models and the Intermodel Uncertainty." *Earth's Future* 12, no. 6: e2023EF004220.

Ma, Y., P. Shi, C. Azorin-Molina, et al. 2024. "Decline in Daily Maximum Wind Speed Over the Tibetan Plateau During 1973–2020: An Examination of Likely Causes." *Climate Dynamics* 62: 10067–10090.

McMahon, R. A., A. M. Peel, L. Lowe, et al. 2013. "Estimating Actual, Potential, Reference Crop and Pan Evaporation Using Standard Meteorological Data: A Pragmatic Synthesis." *Hydrology and Earth System Sciences* 17, no. 4: 1331–1363.

McVicar, T. R., M. L. Roderick, R. J. Donohue, et al. 2012. "Global Review and Synthesis of Trends in Observed Terrestrial Near-Surface Wind Speeds: Implications for Evaporation." *Journal of Hydrology* 416-417: 182–205.

McVicar, T. R., T. G. Van Niel, M. L. Roderick, et al. 2010. "Observational Evidence From Two Mountainous Regions That Near-Surface Wind Speeds Aredeclining More Rapidly at Higher Elevations Than Lower Elevations: 1960-2006." *Geophysical Research Letters* 37, no. 6: L06402.

New, M., D. Lister, M. Hulme, and I. Makin. 2002. "A High-Resolution Data Set of Surface Climate Over Global Land Areas." *Climate Research* 21: 1–25.

Overland, J. E., and M. Wang. 2010. "Large-Scale Atmospheric Circulation Changes Are Associated With the Recent Loss of Arctic Sea Ice." *Tellus. Series A, Dynamic Meteorology and Oceanography* 62, no. 1: 1–9.

Paik, S., and S. K. Min. 2020. "Quantifying the Anthropogenic Greenhouse Gas Contribution to the Observed Spring Snow-Cover Decline Using the CMIP6 Multimodel Ensemble." *Journal of Climate* 33, no. 21: 9261–9269.

Pan, R., W. Li, Q. Wang, et al. 2023. "Detectable Anthropogenic Intensification of the Summer Compound Hot and Dry Events Over Global Land Areas." *Earth's Future* 11, no. 6: e2022EF003254.

Pithan, F., and T. Mauritsen. 2014. "Arctic Amplification Dominated by Temperature Feedbacks in Contemporary Climate Models." *Nature Geoscience* 7, no. 3: 181–184.

Pryor, S. C., and R. J. Barthelmie. 2021. "A Global Assessment of Extreme Wind Speeds for Wind Energy Applications." *Nature Energy* 6: 268–276.

Qian, C., and X. Zhang. 2015. "Human Influences on Changes in the Temperature Seasonality in Mid- to High-Latitude Land Areas." *Journal of Climate* 28, no. 15: 5908–5921.

Screen, J., and I. Simmonds. 2010. "The Central Role of Diminishing Sea Ice in Recent Arctic Temperature Amplification." *Nature* 464: 1334–1337.

Seneviratne, S., M. Donat, A. Pitman, R. Knutti, and R. L. Wilby. 2016. "Allowable CO_2 Emissions Based on Regional and Impact-Related Climate Targets." *Nature* 529: 477–483.

Seong, M. G., S. K. Min, Y. H. Kim, X. Zhang, and Y. Sun. 2021. "Anthropogenic Greenhouse Gas and Aerosol Contributions to Extreme Temperature Changes During 1951-2015." *Journal of Climate* 34, no. 3: 857–870.

Shen, C., J. Zha, Z. Li, et al. 2022. "Evaluation of Global Terrestrial Near-Surface Wind Speed Simulated by CMIP6 Models and Their Future Projections." *Annals of the New York Academy of Sciences* 15, no. 1: 249–263.

Shi, Y., M. Yu, A. Erfanian, and G. Wang. 2018. "Modeling the Dynamic Vegetation–Climate System Over China Using a Coupled Regional Model." *Journal of Climate* 31, no. 15: 6027–6049.

Song, L., Q. Zhuang, Y. Yin, X. Zhu, and S. Wu. 2017. "Spatio-Temporal Dynamics of Evapotranspiration on the Tibetan Plateau From 2000 to 2010." *Environmental Research Letters* 12, no. 1: 014011.

Tian, Q., G. Huang, K. Hu, and D. Niyogi. 2019. "Observed and Global Climate Model Based Changes in Wind Power Potential Over the Northern Hemisphere During 1979–2016." *Energy* 167: 1224–1235.

Vautard, R., J. L. Cattiaux, P. Yiou, J. Cattiaux, J.-N. Thépaut, and P. Ciais. 2010. "Northern Hemisphere Atmospheric Stilling Partly Attributed to an Increase in Surface Roughness." *Nature Geoscience* 3: 756–761.

Vavrus, S. 2004. "The Impact of Cloud Feedbacks on Arctic Climate Under Greenhouse Forcing." *Journal of Climate* 17, no. 3: 603–615.

Wan, H., X. Zhang, F. Zwiers, and S. K. Min. 2015. "Attributing Northern High-Latitude Precipitation Change Over the Period 1966-2005 to Human Influence." *Climate Dynamics* 45: 1713–1726.

Wang, R., B. Liu, H. Li, et al. 2017. "Variation of Strong Dust Storm Events in Northern China During 1978–2007." *Atmospheric Research* 183: 166–172.

Wang, Y., P. Yan, F. Ji, B. Huang, P. Fan, and G. Feng. 2023. "Anthropogenic Contribution to the Rapid Warming Over the Tibetan Plateau." *Climate Dynamics* 61: 329–339.

Wu, F., Q. You, N. Pepin, et al. 2025. "Quantifying Processes of Winter Daytime and Nighttime Warming Over the Tibetan Plateau." *Climate Dynamics* 63: 9.

Wu, J., and X. Gao. 2013. "A Gridded Daily Observation Dataset Over China Region and Comparison With the Other Datasets." *Chinese Journal of Geophysics* 56, no. 4: 1102–1111 (in Chinese).

Wu, J., X. Gao, F. Giorgi, and D. Chen. 2017. "Changes of Effective Temperature and Cold/Hot Days in Late Decades Over China Based on a High Resolution Gridded Observation Dataset." *International Journal of Climatology* 37, no. Suppl. 1: 788–800.

Wu, J., Y. Shi, and Y. Xu. 2020. "Evaluation and Projection of Surface Wind Speed Over China Based on CMIP6 GCMs." *Journal of Geophysical Research: Atmospheres* 125, no. 22: e2020JD033611.

Wu, J., J. Zha, D. Zhao, and Q. Yang. 2018. "Changes in Terrestrial Near-Surface Wind Speed and Their Possible Causes: An Overview." *Climate Dynamics* 51: 2039–2078.

Xiang, Y., T. Wang, H. Wang, and H. Xu. 2024. "Influence of the Pacific Decadal Oscillation on Winter Temperatures and Precipitation Over the Southern Tibetan Plateau." *Journal of Geophysical Research: Atmospheres* 129, no. 6: e2023JD038653.

Xu, H., H. Chen, and H. Wang. 2022. "Detectable Human Influence on Changes in Precipitation Extremes Across China." *Earth's Future* 10, no. 2: e2021EF002409.

Xu, Y., X. J. Gao, Y. Shen, et al. 2009. "A Daily Temperature Dataset Over China and Its Application in Validating a RCM Simulation." *Advances in Atmospheric Sciences* 26: 763–772.

Yang, K., H. Wu, J. Qin, C. Lin, W. Tang, and Y. Chen. 2014. "Recent Climate Changes Over the Tibetan Plateau and Their Impacts on Energy and Water Cycle: A Review." *Global and Planetary Change* 112: 79–91.

You, Q. L., Z. Cai, N. Pepin, et al. 2021. "Warming Amplification Over the Arctic Pole and Third Pole: Trends, Mechanisms and Consequences." *Earth-Science Reviews* 217: 103625.

You, Q. L., S. C. Kang, W. A. Flugel, et al. 2010. "Decreasing Wind Speed and Weakening Latitudinal Surface Pressure Gradients in the Tibetan Plateau." *Climate Research* 42: 57–64.

Zeng, Z., A. D. Ziegler, T. Searchinger, et al. 2019. "A Reversal in Global Terrestrial Stilling and Its Implications for Wind Energy Production." *Nature Climate Change* 9: 979–985.

Zha, J., T. Chuan, J. Wu, et al. 2024. "Attribution of Terrestrial Near-Surface Wind Speed Changes Across China at a Centennial Scale." *Geophysical Research Letters* 51, no. 7: e2024GL108241.

Zha, J., J. Wu, and D. M. Zhao. 2017. "Effects of Land Use and Cover Change on the Near-Surface Wind Speed Over China in the Last 30 Years." *Progress in Physical Geography* 41: 46–67.

Zhang, G. F., C. Azorin-Molina, D. Chen, et al. 2024. "Variability and Trends of Near-Surface Wind Speed Over the Tibetan Plateau: The Role Played by the Westerly and Asian Monsoon." *Advances in Climate Change Research* 15, no. 3: 525–536.

Zhang, L., and T. Li. 2016. "Relative Roles of Anthropogenic Aerosols and Greenhouse Gases in Land and Oceanic Monsoon Changes During Past 156 Years in CMIP5 Models." *Geophysical Research Letters* 43, no. 10: 5295–5301.

Zhang, M., Y. Gao, M. Ting, Y. Yu, and G. Wang. 2024. "Land-Use Induced Changes in Extreme Temperature Predominantly Influenced by Downward Longwave Radiation." *Communications Earth & Environment* 5: 758.

Zhang, Y., L. N. Gao, L. J. Cao, et al. 2020. "Decreasing Atmospheric Visibility Associated With Weakening Winds From 1980 to 2017 Over China." *Atmospheric Environment* 224: 117314.

Zhou, X., K. Yang, and Y. Wang. 2018. "Implementation of a Turbulent Orographic Form Drag Scheme in WRF and Its Application to the Tibetan Plateau." *Climate Dynamics* 50: 2443–2455.

Zhu, L., G. Huang, G. Fan, and W. Hua. 2022. "Influence of Anthropogenic Activities on Elevation-Dependent Weakening of Annual Temperature Cycle Amplitude Over the Tibetan Plateau." *Geophysical Research Letters* 49, no. 10: e2021GL095494.